

CUSZ(x): Optimizing Error-Bounded Lossy Compression for Scientific Data on GPUs

Jiannan Tian,^{*} Sheng Di,[†] Xiaodong Yu,[†] Cody Rivera,[§] Kai Zhao,[‡] Sian Jin,^{*}
Yunhe Feng,[¶] Xin Liang,^{||} Dingwen Tao,^{*} Franck Cappello[†]

^{*}Washington State University, Pullman, WA, USA

[†]Argonne National Laboratory, Lemont, IL, USA

[‡]University of California, Riverside, Riverside, CA, USA

[§]University of Alabama, Tuscaloosa, AL, USA

[¶]University of Washington, Seattle, WA, USA

^{||}Missouri University of Science and Technology, Rolla, MO, USA

Abstract—Error-bounded lossy compression is a critical technique for significantly reducing scientific data volumes. With ever-emerging heterogeneous HPC architecture, GPU-accelerated error-bounded compressors (such as CUSZ and cuZFP) have been developed. However, they suffer from either low performance or low compression ratios. To this end, we propose CUSZ(x) to target both high compression ratio and throughput. We identify that data sparsity and data smoothness are key factors for high compression throughput. Our key contributions in this work are fourfold: (1) We propose an efficient compression workflow to adaptively perform run-length encoding and/or variable-length encoding. (2) We derive Lorenzo reconstruction in decompression as multidimensional partial-sum computation and propose a fine-grained Lorenzo reconstruction algorithm for GPU architectures. (3) We carefully optimize each of CUSZ’s kernels by leveraging state-of-the-art CUDA parallel primitives. (4) We evaluate CUSZ(x) using seven real-world HPC application datasets on V100 and A100 GPUs. Experiments show CUSZ(x) improves the compression performance and ratios by up to 18.4× and 5.3×, respectively, over CUSZ on the tested datasets.

I. INTRODUCTION

Large-scale scientific applications for advanced instruments produce extremely large volumes of data every day for post hoc analysis. For instance, Hardware/Hybrid Accelerated Cosmology Code (HACC) [1, 2] may produce petabytes of data in hundreds of snapshots when simulating 1 trillion particles. It could be very inefficient to store such a large amount of data, especially in situations with relatively low I/O bandwidth on the parallel file system (PFS) [3, 4].

Data reduction is becoming an effective method to resolve the big-data issue for scientific research. Although traditional lossless data reduction methods such as data deduplication and lossless compression can guarantee no information loss, they suffer from very limited compression ratios on scientific datasets. Specifically, deduplication usually reduces the scientific data size by only 20%~30% [5], and lossless compression generally only achieves a compression ratio of up to about 2:1 [6]. This is far lower than the scientists’ desired compression ratios (e.g., 10:1 [7]).

To address the low compression ratio issue, error-bounded lossy compressors have been developed for years. Not only can error-bounded lossy compressors get very high compression ratios (such as 100+) [3, 8, 9, 10], but they can strictly control the data distortion based on the user-required error bound.

A qualified lossy compressor designed for scientific data reduction should address three primary concerns: (1) high fidelity preservation, (2) high compression ratio, and (3) high throughput. Most of the existing error-bounded lossy compressors (such as SZ [8, 9], FPZIP [11], ZFP [10]), however, are mainly designed for CPU architectures, which cannot adapt to the high throughput requirement. For example, X-ray imaging data could be generated on advanced instruments such as the LCLS-II laser [12] with an extremely high data acquisition rate (such as 250GB/s [7]). As such, high compression throughput is very critical to storing the extremely large amount of data efficiently for scientific projects.

Currently, several GPU-based error-controlled lossy compressors (such as CUSZ [13] and cuZFP [14]) have been developed, but they suffer from either sub-optimal compression throughput or low compression ratios. For instance, CUSZ can achieve much higher compression ratios than cuZFP, but its performance is substantially limited by the Huffman encoding stage and dictionary encoding step [15]. However, the high compression ratios of SZ/CUSZ significantly depend on Huffman encoding and dictionary encoding, because the output of the prediction-and-quantization step in SZ/CUSZ is often composed of a large amount of repeated symbols.

In this paper, we propose an efficient compression framework (called CUSZ(x)) based on the CUSZ framework, which can get both high compression ratio and high throughput on GPUs. The notation “(x)” in CUSZ(x) indicates that this new compression method is specifically optimized for high performance in compression and decompression on the latest GPU architecture (i.e., NVIDIA’s Ampere architecture).

It is challenging to develop an efficient GPU-based error-bounded lossy compressor that can achieve both high compression ratios and high throughput. On the one hand, in order to develop efficient GPU code, one has to ensure that the workload can be executed by as many GPU threads as

Corresponding author: Dingwen Tao (dingwen.tao@wsu.edu), School of EECS, Washington State University, Pullman, WA 99164, USA.

possible in parallel. Moreover, the architecture/characteristics of GPU accelerators (such as coherence, divergence issues, bank conflicts, use of shared memory, use of registers) have to be coped with very carefully to get the optimal performance. On the other hand, the state-of-the-art error-bounded lossy compressors (such as SZ [3, 8, 9]) often rely on Huffman encoding and dictionary encoding, which are procedures that contain substantial data dependencies. These dependencies make them very hard to parallelize on GPUs efficiently. For example, before performing Huffman encoding, a Huffman tree has to be built based on the code-frequency histogramming, which has a significant data dependency inside. The CUSZ code just used one single GPU thread to do this work for simplicity. Moreover, it is fairly non-trivial to design an efficient parallel code for the dictionary encoding because of the intrinsic dependency in its repeated sequence search. CUSZ leaves this part to CPU, which may suffer from significant overhead. Our key contributions proposed particularly in CUSZ(x) are summarized as follows.

- We design an adaptive compression workflow to perform run-length encoding and/or variable-length encoding (i.e., Huffman encoding) on GPUs. We exploit an effective condition to determine when the run-length encoding should be applied for improving compression ratio: i.e., when the average Huffman bit-length is no greater than 1.09.
- We identify and prove that the first-order Lorenzo reconstruction in decompression can be converted to a multi-dimensional partial-sum computation. We propose a fine-grained Lorenzo reconstruction algorithm based on multi-dimensional partial-sum and modified quantization scheme. Such a design can fully parallelize the decompression operation at the GPU-thread level such that the overall decompression throughput can be improved significantly.
- We develop some optimization strategies to boost compression performance and scalability. For instance, we carefully optimize each kernel in compression considering CUDA architecture (e.g., reducing global memory accesses) to improve the compression throughput. We also leverage the state-of-the-art NVIDIA::cub parallel primitives [16] to enhance the decompression scalability and throughput.
- We evaluate CUSZ(x) with seven real-world HPC application datasets from public *Scientific Data Reduction Benchmarks* [17] on two state-of-the-art GPUs—V100 and A100. Experiments show that CUSZ(x) improves the compression performance and ratios by up to 18.4× and 5.3×, respectively, over CUSZ on the tested datasets.
- We conclude that with the advancement of GPU architecture, CUSZ(x) can benefit more from the memory bandwidth improvement than the peak FLOPS improvement, and provide valuable insights for software and application R&D toward the exascale era.

II. BACKGROUND AND RESEARCH MOTIVATION

In this section, we introduce the background of CUSZ (the GPU version of SZ [9]) [13] and our research motivation.

1) *Background of CUSZ*: Unlike the CPU-based version of SZ that has only four steps (prediction, quantization, Huffman encoding, and dictionary encoding), CUSZ involves 9 steps to adapt to the GPU architecture. Specifically, Step 1 is splitting the whole dataset into multiple blocks, each of which will be compressed independently. This design is for the purpose of executing coarse-grained decompression. Upon splitting blocks, CUSZ’s compression adopts a dual-quantization scheme (including three steps: prequantization¹, prediction, and postquantization), which can entirely remove the data dependency for the Lorenzo prediction. Then, Step 5 adopts a parallel histogramming to compute the frequencies of the quant-codes. Step 6 builds a canonical Huffman codebook [13] based on the histogram/frequency vector. Step 7 performs the Huffman encoding over the quant-codes. Step 8 concatenates all the Huffman codes (called deflating) on GPUs, which will be further compressed by a dictionary encoder (Zstd [18]) on CPUs in Step 9. The decompression is the simple reversed procedure of the compression. We refer readers to the CUSZ paper [13] for more details.

For compression, Step 6 and 9 are the main bottlenecks, because Step 5 has to be executed sequentially with a single GPU thread, and designing an efficient multi-thread GPU algorithm for dictionary encoding is non-trivial.

For decompression, the first step (i.e., dual-quantization) is the main bottleneck since the decompression cannot adopt the prequantization step. Specifically, in the decompression stage, the data values have to be reconstructed one by one, according to the Lorenzo predictor². To address this issue, CUSZ adopts a coarse-grained parallel method instead: letting a GPU thread handle one independent data block in parallel. However, such design suffers from a low performance due to the low utilization of massive parallelism on GPUs. In addition to Step 1, Step 9 is another significant bottleneck because the dictionary decoding is also very hard to parallelize on GPUs because of its intrinsic data dependency.

2) *Research Motivations*:

Limitation of CUSZ’s Compression Ratio Unlike fully fledged CPU-based data compressors such as gzip (an implementation of the DEFLATE algorithm including LZ77 and variable-length encoding, “VLE”), the GPU-based lossy compressor CUSZ only leverages variable-length encoding (i.e., Huffman coding) to compress prediction-error correction codes (i.e., quant-codes). Because at least 1-bit codeword needs to be used to represent the original symbol, CUSZ can achieve up to 32× or 64× of compression ratios by only using Huffman coding, which disregards the repeated pattern that may exist in the symbol sequence. Hence, there is a gap between CUSZ and CPU-SZ in compression ratio due to lack of pattern-finding-based coding methods.

¹All data points are quantized based on their original values before the data prediction step.

²Lorenzo predictor predicts the data values based on a high-order data approximation formula: e.g., $X(i, j) = X(i - 1, j) + X(i, j - 1) - X(i - 1, j - 1)$ for 2D dataset, where $X(i, j)$ refers to the value of the data point (i, j) in the dataset

| | HACC | | | Hurricane | | |
|------|-----------|-----------|------------|-----------|-----------|------------|
| | <i>qq</i> | <i>qh</i> | <i>qhg</i> | <i>qq</i> | <i>qh</i> | <i>qhg</i> |
| 1e-2 | 22.72 | 20.33 | 31.02 | 43.67 | 24.80 | 58.76 |
| | 1.1× | 1.0× | 1.5× | 1.8× | 1.0× | 2.4× |
| 1e-3 | 7.58 | 9.51 | 10.01 | 18.41 | 17.04 | 24.65 |
| | 0.8× | 1.0× | 1.1× | 1.1× | 1.0× | 1.4× |
| 1e-4 | 3.89 | 4.82 | 5.01 | 10.31 | 9.76 | 12.99 |
| | 0.8× | 1.0× | 1.0× | 1.1× | 1.0× | 1.3× |
| | CESM | | | Nyx | | |
| | <i>qq</i> | <i>qh</i> | <i>qhg</i> | <i>qq</i> | <i>qh</i> | <i>qhg</i> |
| 1e-2 | 61.21 | 24.24 | 75.50 | 118.94 | 30.24 | 164.39 |
| | 2.5× | 1.0× | 3.1× | 3.9× | 1.0× | 5.4× |
| 1e-3 | 20.78 | 18.38 | 28.13 | 28.25 | 23.92 | 40.17 |
| | 1.1× | 1.0× | 1.5× | 1.2× | 1.0× | 1.7× |
| 1e-4 | 9.98 | 10.29 | 12.50 | 12.87 | 15.27 | 17.95 |
| | 1.0× | 1.0× | 1.2× | 0.8× | 1.0× | 1.2× |

TABLE I: Averaged compression ratios (per dataset) of different compression schemes on 109 fields of 4 datasets with 3 error bounds of 10^{-2} , 10^{-3} , 10^{-4} (relative to value range). *q* denotes quant-code as starting point, *h* denotes customized variable-length encoding (multibyte-symbol Huffman coding), *g* denotes gzip-featured scheme. “*ab*” denotes scheme *a* precedes scheme *b*.

TABLE I shows the compression ratio variances by applying the CUSZ workflow followed by gzip. *q*, *h*, *g* denote *prediction-quantization*, *multibyte Huffman coding*, *gzip*, respectively, and the letter sequence indicates the order of processes (e.g., *qh* indicates that *h* comes after *q*). However, this additional gzip so far does not exist in CUSZ but can demonstrate that the potentially achievable compression ratio by exploiting the repeated symbol pattern. More specifically, by changing the error bound from 10^{-4} to 10^{-2} , Lorenzo predictor generates the intermediate quant-codes that exhibit stronger repeated patterns, as indicated in *qh*. For example, when changing from *qh* to *qhg*, HACC data shows only $1.04\times$ improvement in compression ratio under the error bound of 10^{-4} , while the compression ratio is improved by $1.52\times$ under the error bound of 10^{-2} . We use the compression ratio of this *qhg* as a reference in the following discussion.

Limitation of CUSZ’s Decompression Performance CUSZ follows CPU-SZ’s scheme to sequentially reconstruct the prediction values in decompression (per data chunk). Specifically, the reconstruction value of one point must be calculated based on its preceding values that are fully reconstructed. As a result, this scheme is naturally implemented in a sequential manner because of data dependency. Moreover, since both CPU-SZ and CUSZ store the unpredicted data and the prequantized data, separately, it introduces an extra handling step involving if-branch in decompression, which impedes fine-grained data-parallelization. In addition, compared to CUSZ’s compression kernel, its decompression kernel’s throughput is relatively low [13]. In particular, the Lorenzo construction kernel can achieve the same order of magnitude of throughput as memory copy [13], while the Lorenzo reconstruction kernel has one order of magnitude less in throughput. All above prevent CUSZ from wider use scenarios such as in-situ/in-memory compression.

Importance of Lorenzo Predictor The modular design of SZ framework enables adaptively adopt various predictors for different scientific uses. Among all predictors, the first-order Lorenzo predictor plays an important role in the SZ compression framework (the default predictor), since it achieves

relatively low prediction error in most cases, as proved in prior works [3, 9, 19].

Overall, in this work we endeavor to significantly boost compression ratio and (de)compression performance of CUSZ (e.g., Lorenzo reconstruction kernel) by developing a series of optimization techniques to address the above issues.

III. COMPRESSIBILITY-AWARE COMPRESSION FRAMEWORK OVER GPU

In this paper, we propose a compressibility-aware framework that can improve compression ratio significantly in many cases. The key design motivation is based on our in-depth analysis of the CUSZ’s principle and careful observation of CUSZ’s performance and compression ratio. According to CUSZ’s design [13], all the compression computations must be executed on GPUs for high-performance purpose, leading to that the compression ratios no greater than 32 (for single-precision) or 64 (for double-precision). This is due to the lack of dictionary coding or other pattern-finding-based coding methods. We note that if “being smooth enough” is satisfied, we can apply the alternative technique run-length encoding (“RLE”) to achieve higher compression ratio, while maintaining 1) the same data quality and 2) a comparable throughput. Note that below we use *default workflow* to denote “Lorenzo + multibyte VLE” and *RLE-based workflow* to denote “Lorenzo + RLE” with optional VLE.

In the following sections, we first present the overview of our compressibility-aware design, and then describe our optimization strategies in detail. Figure 1 presents the overview of our new compression framework (i.e., CUSZ(X)) versus the old compression framework (i.e., CUSZ). As shown in the figure, the adaptivity is reflected in three workflow paths.

A. Compressibility

1) *Source of Compressibility*: The rationale for SZ framework to achieve high compression is twofold. First, integer data are easier to compress than IEEE-754 floating-point data. Non-special float-type number (e.g., non-zero) requires full 32 bits to represent any arbitrary number (even integer). SZ’s prediction-quantization step transforms prediction errors into quant-codes in integer and eliminates the randomness majorly from floating-point mantissa. Second, the quant-codes within a pre-defined range would be further losslessly compressed, while the out-of-range quant-code are marked as *outliers*. Then, we enumerate the in-range quant-codes (as symbols in Huffman codebook key-values or bin numbers) in histogram. Unlike byte-based generic compression methods, $n_{\text{enum}} = 2^{\lceil \log \text{range} \rceil}$ can overflow a single byte, thus, multiple bytes are used to represent a symbol (the number of multiple bytes is determined by $\lceil n_{\text{enum}}/8 \rceil$). This ensures that the enumeration reflects the distribution of quant-codes, e.g., the most frequent code uses the least number of bits in encoding.

2) *Referenced Compression Ratio*: As shown in TABLE I, we enumerate the lossless compression techniques that are currently used in CPU-SZ and CUSZ, and show quantitative examples consequential compression ratio with different error

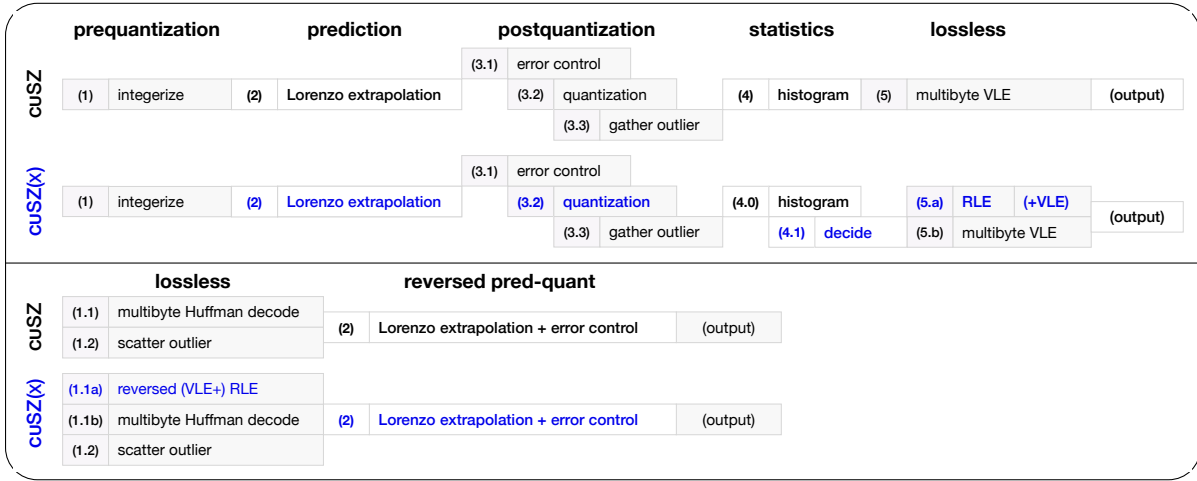


Fig. 1: Compression (top) and decompression (bottom) workflows of the original CUSZ and our CUSZ(x). Our adaptive solution toward better throughput and compression ratio, featuring 2 workflow paths. The solid lines indicate that memory copy is involved while dotted lines indicate decision making with minimal data used. For simplicity, alphabetic letters in parentheses indicate memory copy source (left) and target (right). The changes from CUSZ to CUSZ(x) are marked with blue color.

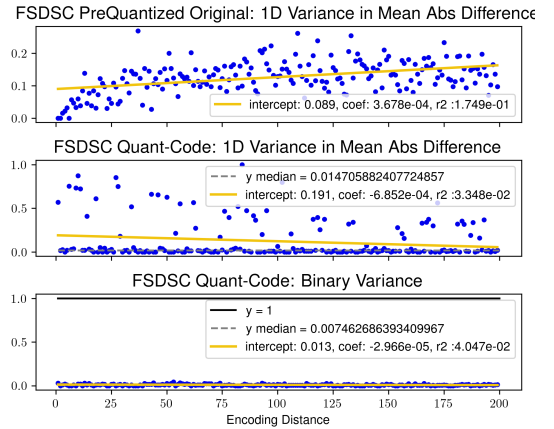
bounds. In the table, *qg* serves to demonstrate a presumed sub-optimal scenario; the singlebyte interpretation (from generic CPU compressor) does not indicate the most likely quant-code and hence hurt the compressibility. *h* indicates multibyte symbol enabled Huffman coding that is used in both CPU-SZ and CUSZ. *qh* indicates CUSZ compression schemes that are totally done on GPUs while *qhg* adds an additional gzip to exhibit the highest possible compression ratio, which is archived by CPU-SZ. We will use the compression ratio from *qhg* as a reference in the following discussion.

3) *Data Feature Awareness*: Even though appending another pattern-exploiting stage to CUSZ would result in optimal compression ratio, it can severely affect the throughput since gzip takes place on host. This motivates us to visit the data features that can favor compressibility. On the other hand, the repeated pattern is non-trivial to utilize. This is because pattern finding is usually implemented as dictionary coding with access to variable-length bits and the reported low throughput. For instance, LZ4 (featuring relatively high throughput [20] compared to CUSZ) would not fit into the use scenarios where in situ big data processing is on demand.

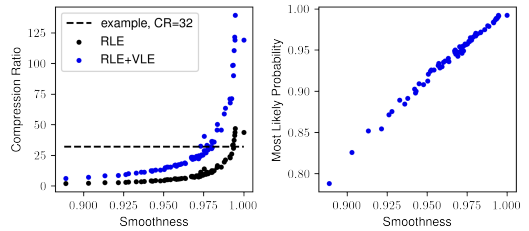
In this work, we propose a solution to exploit the repeated data pattern by leveraging the indication of data smoothness. Specifically, the error compensation in terms of quant-code becomes zero when the predicated value is less than one unit of *eb* away from the original value, and the non-zero quant-codes can be scattered across the whole dataset. We consider that the quant-codes are smooth when they are *locally* continuous with the same values, and propose to use run-length encoding to explore the data patterns that may exist in these quant-codes.

In addition to the new handling, we can append an additional Huffman encoding as an option, which further brings steadily $2\times$ to $3\times$ compression ratio on the top of the RLE compression ratio gain. Our design goal is to push the compression ratio beyond the original $32\times$ for float (or $64\times$ for double); considering the throughput, compressing the metadata of RLE

output is optional and by default omitted disabled in GPU processing. We further expand the criteria and the uses of RLE in §III-B.



(a) Smoothness against encoding distance (CESM FSDSC at 1e-2).



(b) Smoothness-Probability of the most likely symbol relationship.

Fig. 2: Smoothness of prequantized data and quant-code, and smoothness-probability of the most likely symbol relationship can help determine when to use RLE. For example, a threshold compression ratio can set to 32 to find a desired smoothness, and the smoothness can be directed to the probability of the most likely symbol.

B. Smoothness and Run-Length Encoding

RLE (first introduced in [21]) is a form of lossless compression in which sequences of consecutive same-value data elements are stored as value-count tuples. Such kind of sequences are called runs of data. For example, “aabccccaa” is stored as “(a,2)(b,1)(c,5)(a,2)”. Such kind of encoding as a simplistic pattern-finding-based coding method can be in place of others in favor of high throughput on GPUs.

Without prefix property used by Huffman coding, length of runs must be recorded as metadata, introducing an extra overhead. This immediately leaves the questions: (1) how to model the compressibility, and (2) when to use RLE. We identify that histogram and madogram (a variogram variant) can help make decision: madogram is sufficient to reveal the underlying reason why RLE can perform well, while histogram is easy to perform and can converge to indicate the satisfaction of performing RLE.

1) *Estimation from Histogram*: We first discuss the data features for RLE and VLE based on the histogram. The entropy value of the histogram is calculated as $H(X) = -\sum p_i \log_2 p_i$, where p_i is the probability of the i -th symbol. We use $\langle b \rangle$ to denote the average Huffman codeword bit-length. We use R (redundancy) to denote the discrepancy between $\langle b \rangle$ and entropy $H(X)$ (i.e., $R = \langle b \rangle - H(X)$). Without building the Huffman tree, we can estimate the upper and lower bound of the average bit-length (i.e., $\langle b \rangle = R + H(X)$) by using the entropy value and the probability of the most likely symbol (i.e., p_1). The lower bound of R is given by [22] (under the restriction of $p_1 > 0.4$):

$$R \geq \tilde{R} = 1 - H(p_1, 1 - p_1),$$

where $H(p_1, 1 - p_1) = p_1 \log_2 \frac{1}{p_1} + (1 - p_1) \log_2 \frac{1}{1 - p_1}$.

The upper bound is given by $p_1 + 0.086$ (no restriction) [23]. In the following text, we make use of these estimations before performing VLE (which follows RLE).

2) *Modeling RLE Compressibility*: Due to the obvious overhead, RLE would be used when the data is *smooth enough*. However, the aforementioned histogram cannot reflect the data smoothness. In general, the encoding iteration goes over data is much sensitive to and directly impacted by the local smoothness, which histogram does not reflect. This is because a locally smooth datum can have similar histogram to that of a locally rougher one. Considering that RLE discontinues when hitting a next different data value, the data smoothness can also be measured in binary manner.

The method of variogram [24] inspires us to derive a new scheme to measure the smoothness. Variogram (i.e., general-purpose multidimensional data variance) is one of the most effective metrics to reveal spatial data variance-distance relationship based on sampling method. Its theoretical form is

$$2\gamma(\mathbf{s}_1, \mathbf{s}_2) = \text{var}(Z(\mathbf{s}_1) - Z(\mathbf{s}_2)) = E \left[(Z(\mathbf{s}_1) - Z(\mathbf{s}_2))^2 \right],$$

where $Z(\mathbf{s})$ is a spatial random field. Considering the encoding iteration is unidimensional, we substitute the power description $(Z(\mathbf{s}_1) - Z(\mathbf{s}_2))^2$ with the absolute difference $|Z(\mathbf{s}_1) - Z(\mathbf{s}_2)|$

to form the *madogram*. Also, note that one *RLE run* discontinues when the data value differs from the current one, we further adjust the absolute difference to binary difference, defined it as

$$\text{binary variance/roughness} = \begin{cases} 0 & v_{\text{current}} = v_{\text{next}} \\ 1 & v_{\text{current}} \neq v_{\text{next}} \end{cases},$$

and smoothness is defined as $(1 - \text{binary roughness})$. Given the $\mathcal{O}(n^2)$ nature of enumerating pairwise variances, empirical madogram method is conducted by using a offline sampling scheme. More specifically, given a sufficiently large number sampling number N and a maximum distance of measurement $D_{\text{max}} = 200$, we form the pair $(a, a + d)$, where a is randomly selected from the whole data field, and $d = \text{rand}(1, 200)$ (suppose $(a + d)$ is in the data range). The summed variance of each distance is averaged by its corresponding count. The averaged binary variance $v(d)$ can be used to measure the roughness, and $1 - v(d)$ can be used to measure the smoothness.

We first show the madogram of the prequantized original data and quant-code in absolute difference and the madogram of quant-code using binary variance in Fig.2. Fig.2a shows that quant-code is smoother with less variance than the prequantized original data. This indicates that the prediction-quantization scheme can much decrease the data representative bits by using much less integer numbers and achieve high data reduction ratio. The third part of Fig.2a indicates that quant-code can forward-encode from a fixed starting point with almost equal roughness at an arbitrary distance from the starting point. Hence, at a stable rate of roughness, RLE can continue. The next step is to determine the threshold. Fig.2b shows that with binary variance we can relate (1) data continuity/smoothness and the compression ratio (CR) and (2) data smoothness and the probability of the most likely symbol (p_1). With (1), for example, a simplistic case is to set a CR threshold at 32 and look up the smoothness for RLE or RLE+VLE. With (2), p_1 can determine compression ratios of both the proposed RLE workflow and VLE in CUSZ and be used to select from the two workflows. For example, FSDSC has an RLE-CR above 25 while CUSZ-VLE-CR is 26~29 \times . Note that 1) there is overhead of chunkwise metadata from CUSZ-VLE (the final CR is 23.88) and 2) additional VLE after RLE can provide steady 3 \times more CR in general (estimated from the corresponding histogram), making the accumulated CR above 70 \times in this case. Thus, we can use p_1 and entropy from histogram to choose the case in which RLE can achieve higher compression ratio and comparable throughput.

IV. PERFORMANCE OPTIMIZATION

In this section, we present our optimization strategies, featuring (1) performance improvements on *each* kernel in compression, and (2) a new high-performance Lorenzo reconstruction kernel in decompression.

A. Compression Optimization

1) *Dual-Quantization*: In the original SZ algorithm, the quant-code used in variable-length coding is generated from

the predict-quant procedure, requiring in situ (compression-time) data *reconstruction*, which causes *read-after-write* dependency in compression. Specifically, for any data point at $(k-1)$ -th iteration in compression, its prediction error is first calculated as $e_{k-1}^\circ = d_{k-1} - p_{k-1}^\circ$ (where p_{k-1} is the predicted value based on the reconstructed data generated in the preceding iterations) and then integerized as quant-code q_{k-1} based on the user-specified error bound eb . After that, the compression-time reconstructed data $d_{k-1}^{\circ*}$ is computed through the *error compensation* $e_{k-1}^{\circ*}$, which is transformed from q_{k-1}° . From the saved quant-code q_{k-1}° , the decompression-time reconstruction replays the *q-e-d* procedure to ensure the error-boundedness. Such compression-time reconstruction incurs loop-carried RAW dependency [13]. CUSZ resolved this tight dependency by prioritizing the integerization via two-phase prediction-quantization, called DUAL-QUANTIZATION (or DUAL-QUANT):

prequant The integerization is done by $d^\circ = \text{round}\langle d/(2 \cdot eb) \rangle$, where d is the original data value, such that the compression error $|e| = |d - d^\circ \cdot 2eb| < eb$ is guaranteed.

postquant The difference between the prediction p° based on integerized surrounding values and the target integer value d° is rendered as $\delta^\circ = d^\circ - p^\circ$. The quant-code q° is equivalently δ° (represented differently).

CUSZ work noted that it is unnecessary to conduct compression-time reconstruction, because it is deterministic to generate d° via error compensation δ° replayed as $\delta^{\circ*}$ —they are equivalent to q° . As a result, the loop-carried RAW dependency can be eliminated completely.

Moreover, it is worth noting that CUSZ’s method for eliminating RAW dependency also works for CUSZ(x) with Lorenzo predictor. According to Tao et al. [9], the general-form Lorenzo predictor is given by

$$\sum_{0 \leq k_1 \dots k_m \leq n} \left\langle \prod_{j=1}^m (-1)^{k_j+1} \binom{n}{k_j} \right\rangle \cdot d_{x_1-k_1, \dots, x_d-k_d},$$

where $\sum_{0 \leq k_1 \dots k_m \leq n} \left\langle \prod_{j=1}^m (-1)^{k_j+1} \binom{n}{k_j} \right\rangle = 1, \forall d$.

Thanks to DUAL-QUANT, all the coefficients in the formula are integers, and their sum is 1. Thus, the prediction computation consists entirely of integer-based operations (additions and multiplications, *no* division), resulting in a unit weight. Moreover, the data reconstruction based on this is precise and robust with respect to machine ϵ . In addition, as is known, integer is commutative in summation, i.e., $a + b = b + a$, thus given arbitrary numbers of integers, adjusting summation order results in no difference in sum. This property guarantees that our proposed fine-grained Lorenzo reconstruction (will be discussed in §IV-B) can reorder the prediction computation.

2) *Compression Kernel Enhancement*: We mainly focus on optimizing two compression kernels: the Lorenzo construction kernel and the Huffman encoding kernel. Besides coalescing load from and store to DRAM/shared memory, we propose two major strategies to increase the number of thread blocks (or warps) that can run concurrently within one streaming multiprocessor (SM). 1) We coarsen the granularity by assigning more data points to one thread. For example, a 16×16 2D data

chunk is equally split into two groups, each of which traverses over consecutive 8 points along y -direction. Note that the data-thread mapping is not necessarily the same as coalescing load/store. In such manner, it is possible to launch more thread blocks in the same SM to achieve higher occupancy. 2) We exploit register file use and perform in-warp shuffle to exchange data. This is because the extrapolative prediction uses neighboring data points that are largely assigned to the threads, whose index difference is 1. This strategy can decrease the share memory use to launch more warps in the same SM. The comparison between the kernels of CUSZ and our CUSZ(x) is shown in TABLE VII.

B. Decompression Optimization

1) *Modified Quantization Scheme*: In order to enable fine-grained parallel decompression in GPU architectures, quantization scheme in compression needs to be modified in accordance with the Lorenzo reconstruction procedure. In CUSZ, if the error compensation δ° associated with its corresponding prequant-ized d° is out-of-range, d° is stored as an outlier, while 0 is stored as the alternative quant-code. In CUSZ(x), if the compensation δ° is out-of-range, δ° is stored as an outlier (line 7 in Algorithm 1), while the quant-code remains stored in the same way (line 5 in Algorithm 1). Then, the outlier and the quant-code are further processed, i.e., stored directly and compressed losslessly, respectively. During the decompression, the outlier and the quant-code are extracted from the compression archive, i.e., extracted directly and from Huffman decoding, respectively.

During decompression, CUSZ accesses outlier when hitting 0 (the alternative quant-code). However, CUSZ’s coarse-grained reconstruction only exploits the parallelism of GPU but rarely considers dependency, memory access pattern, and computational efficiency. In comparison, by using the modified quantization, CUSZ(x) fuses the quant-code and the outlier before reconstruction (line 12 in Algorithm 1). In such manner, we conduct the reconstruction from the error compensation δ^\bullet without any stall, hence eliminating the dependency that exists in CUSZ’s coarse-grained reconstruction.

2) *Partial-sum-based Lorenzo Reconstruction*: As aforementioned, the first-order Lorenzo prediction is used in CUSZ(x). We can write the $\{1,2,3\}$ -dimension first-order Lorenzo predictors as follows.

$$\begin{aligned} p_{[x]} &= + d_{[x-1]} \\ p_{[y,x]} &= - d_{[y-1,x-1]} + d_{[y-1,x]} + d_{[y,x-1]} \\ p_{[z,y,x]} &= + d_{[z-1,y-1,x-1]} - d_{[z-1,y-1,x]} - d_{[z,y-1,x-1]} + d_{[z,y-1,x]} \\ &\quad - d_{[z-1,y,x-1]} + d_{[z-1,y,x]} + d_{[z,y,x-1]} \end{aligned}$$

In decompression, $d^\bullet = p^\bullet + q^\bullet - r$; after substituting $q^\bullet - r$ with q' , it becomes $d^\bullet = p^\bullet + q'$. Considering the initial condition, i.e., predicting from zeros, the first predicted point is $d_{[0,0]}^\bullet = q'_{[0,0]}$. We observe that an arbitrary point $[y,x]$ is predicted as $\sum_{j=0}^y \sum_{i=0}^x q'_{[j,i]}$. Furthermore, it is easy to prove

Algorithm 1: Lorenzo construction and reconstruction.

```

1 for all  $d \in D$  do ▷ compression
2    $d^\circ \leftarrow d / (2 \times eb)$  ▷ PREQUANT, barrier
3    $p^\circ \leftarrow \ell(d_{\text{SR}}^\circ)$ ,  $\delta^\circ \leftarrow p^\circ - d^\circ$ 
4   if  $\delta^\circ < \text{cap}/2 \equiv \text{radius}$  (in-cap) then ▷ POSTQUANT
5      $q^\circ \leftarrow \text{CAST}<\text{FP2INT}>(\delta^\circ)$ 
6   else
7     outlier  $\leftarrow \delta^\circ$  ▷ remaining fp presence
8   end if
9 end for

10 for dim in  $[x, y, z]$  do ▷ decompression
11   for all  $q^\bullet$  of dim from  $\Delta^\bullet \equiv \Delta^\circ$  do
12      $q' \leftarrow (q^\bullet \oplus \text{outlier}) - \text{radius}$  ▷ fuse into quant.
13      $d^\bullet \leftarrow \sum_{q' \text{ the same axis}} q'$  ▷ inclusive partial-sum
14   end for
15 end for
16 output  $\leftarrow d^\bullet \cdot (2 \times eb)$ 

```

that the below sum-expression holds for the point $[y+1, x+1]$.

$$\begin{aligned}
d_{[y+1, x+1]}^\bullet &= - \sum_{j=0}^y \sum_{i=0}^x q'_{[j, i]} + \sum_{j=0}^y \sum_{i=0}^{x+1} q'_{[j, i]} + \sum_{j=0}^{y+1} \sum_{i=0}^x q'_{[j, i]} + q'_{[y+1, x+1]} \\
&= \sum_{i=0}^y q'_{[j, x+1]} + q'_{[y+1, x+1]} + \sum_{j=0}^{y+1} \sum_{i=0}^x q'_{[j, i]} = \sum_{j=0}^{y+1} \sum_{i=0}^{x+1} q'_{[j, i]}.
\end{aligned}$$

An intuitive demonstration for 2D case is shown in Fig.3a. Note that there is cancellation in the joint summation.

Computation as ND Partial-Sum: An N -D partial sum can be expressed as n -time multi-stripe partial-sum. In the 2D case, the two-time multi-stripe partial-sum is illustrated as below. Suppose there is a b -by- b (e.g., 8-by-8 for demonstration) block and padding zeros on the upper and left sides. The first-time partial-sum is performed through points $d_{[j, 0 \dots b]}$, where there are b parallel 1D partial-sums along x -direction. Given an arbitrary y , the partial-sum at $[y, x]$ is $\sum_{i=0}^x q'_{[y, i]}$. The second-time partial sum is then performed through points $d_{[0 \dots b, i]}$, where there are b parallel 1D partial-sums along y -direction. Despite the implementation, a single-time multi-stripe partial-sum can be done in $\mathcal{O}(\log_2 b)$. Considering the memory access pattern and thread organization, partial-sum along x -direction can be mostly computed by a GPU thread warp. In comparison, y - and z -direction partial sums are beyond thread warps because of the memory access stride (i.e., b and $b \times b$).

3) *Implementation Detail:* We conduct the partial-sum computation within each chunk (i.e., no inter-chunk dependency). To illustrate the effectiveness of the proposed partial-sum solution (“naïve” column in TABLE II), we first have a proof-of-concept implementation using shared memory and map each data point to one thread. This implementation significantly improves the reconstruction performance compared to the coarse-grained reconstruction used in CUSZ. Note that the new reconstruction kernel has a comparable performance with the fine-grained construction kernel in CUSZ (“ref. CUSZ” column). Our proposed fine-grained solution for CUSZ(x) exhibits higher resource utilization than the coarse-grained

parallelization does in CUSZ.

Then, it is worth noting that the arithmetic intensity of the Lorenzo reconstruction kernel is relatively low (i.e., the algorithmic time complexity is linear), which tends to be memory bounded. Thus, we consider the two optimizations for the naïve implementation:

- 1) We tune the access pattern to ensure the coalesced load/store from/to global memory.
- 2) We increase the *sequentiality* to each thread to balance load/store and computation.

By using these optimizations, we form a different thread block management, considering that there is no canonical way to map the thread to the data. Rather, the data-thread mapping is more bottom-up, so the warp convergence needs to be considered first. On the other hand, our problem is more “streaming”-flavored, so there is no much locality that we can exploit during the computation. This is unlike “persisting”-flavored problem such as *gemm*, whose algorithmic complexity tends to be $\mathcal{O}(n^3)$. Therefore, the workflow path of *global-memory* \rightarrow *register* \rightarrow *shared-memory* is not efficient and necessary, when the register file can hold a certain amount of data and perform in-warp operations.

1D Implementation: We attribute the chunkwise partial-sum to 1D BlockScan and implement it using `NVIDIA::cub` library. Warp-stripped load/store from/to global memory is used to ensure the coalesced read/write. We test different sequentialities of each thread with warp/block-wide scan-and-sync employed. We use 256 as 1D chunk size in CUSZ(x) and the `V_x` field in the 1D HACC dataset as an example in TABLE II.

2D Implementation: There is no such direct abstraction, however, for higher-dimensionality partial-sum—the multidimensional use of `cub` is internally linearized to 1D. Thus, we handcraft the 2D reconstruction kernel. We use 16×16 as 2D chunk size in CUSZ(x) (the same as CUSZ). The 1-to-1 thread-data and unconditional use of shared memory (the only explicit cache in GPUs) incurs both low computational utilization of each thread (and hence warp) and underuse of register file. In-warp operations such as `__shfl_up_sync` allow accessing the register in the same warp and hence data exchange without using shared memory. We then specify x -direction as warp-shuffling space while setting sequentiality to y -direction. Each thread holds a $n_{(2)}$ -length thread-private array `tp[]`, in which a fragment of partial-sum is sequentially and trivially done. $\frac{16}{n_{(2)}}$ threads are needed along y -direction to complete a size-16 partial sum. Of the same y , all threads except the last one propagate the last-element value in `tp[]` to all the elements in next thread’s private array, sequentially, using shared memory to exchange. We identify the sequentiality of 8 results in the optimal throughput under such thread block configuration—a $(16, 2, 1)$ -block size comprises of a warp—at 254.2 GB/s on V100 and 508.6 GB/s on V100 with testing on a sample CESM field. The throughputs are comparable to the high-throughput 1D kernel—justifiable across the dimensionality.

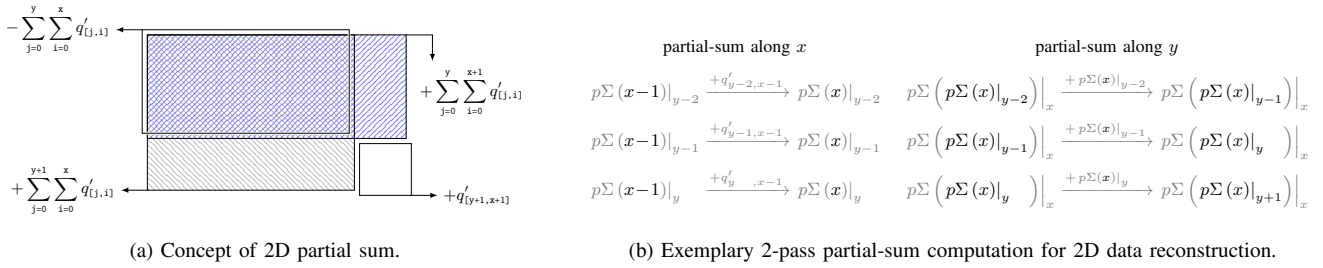


Fig. 3: Example of 2D partial-sum computation for Lorenzo reconstruction in CUSZ(x)'s decompression.

| | | cuSZ [13] | ours (naïve) | ours (optim) | A100 adv. over V100 | |
|-----------|------|--------------|-----------------|-----------------|------------------------|-------|
| 1D (HACC) | A100 | - | 219.8 | +130% | 504.5 | 1.64× |
| | V100 | 16.8 | +1404% | 252.6 | +24% | 313.1 |
| 2D (CESM) | A100 | - | 182.1 | +179% | 508.6 | 2.00× |
| | V100 | 58.5 | +239% | 198.4 | +28% | 254.2 |
| 3D (Nyx) | A100 | - | 147.9 | +174% | 405.1 | 1.70× |
| | V100 | 29.7 | +492% | 175.9 | +35% | 238.1 |

TABLE II: Proof-of-concept throughput (in GB/s) on V100 for 1D, 2D, and 3D. The referenced throughput of CUSZ's Lorenzo reconstruction is across all fields [13]. The table shows one field (i.e., vx in HACC, CLDHGH in CESM, baryon-density in Nyx) for demonstration purpose.

3D Implementation: The 3D problem has an addition to the 2D implementation. Right after the same procedure in 2D case, we append an x - z transposition of the x - and y -direction partial-sum result and repeat the previous x -direction partial-sum (with z -direction data). Based on trials, we identify that the $8\times$ sequentiality results in the best throughput. Yet 3D kernel, due to the longer computational process, does not archive as high throughput as lower dimensionality. Further evaluation and analysis are listed in TABLE VIII in §V.

V. EXPERIMENTAL EVALUATION

In this section, we present our experimental setup (platforms, baselines, and datasets) and our evaluation results.

A. Experimental Setup

1) *Evaluation Platform:* We conduct our experimental evaluation on two HPC systems equipped with NVIDIA Tesla V100 and A100 GPUs³, including ThetaGPU [25] at Argonne Leadership Computing Facility and Longhorn[26] at Texas Advanced Computing Center. More details can be found in the below table.

| | |
|----------|--|
| ALCF | NVIDIA A100, SXM4 variant, CUDA 11.1 |
| ThetaGPU | DRAM 40 GB HBM2e at 1555 GB/s (1.38× V100) |
| | compute 19.49 FP32 TFLOPS (1.73× V100) |
| | host AMD 7532, 32-core, 256 GB, PCIe4 |
| TACC | NVIDIA V100, PCIe variant, CUDA 10.2 |
| Longhorn | compute 14.13 FP32 TFLOPS |
| | host 2 IBM Power9, 40-core, 256GB GB, NVLink |

TABLE III: Our evaluation platforms.

³We note that the PCIe A100 holds a marginal (30%) less throughput than the SXM4 A100. In this work, we use the SXM4 variant for evaluation.

2) *Baselines:* We compare our CUSZ(x) with multiple baselines. Specifically, 1) we compare CUSZ(x) with CUSZ in terms of our optimized kernels (i.e., Lorenzo construction, Huffman encoding, Lorenzo reconstruction), 2) we compare CUSZ(x) on A100 versus on V100, and 3) we compare CUSZ(x)'s RLE-based compression workflow with CUSZ's Huffman-coding-based compression workflow.

3) *Test Datasets:* We conduct our evaluation and comparison based on seven typical real-world HPC simulation datasets of each dimensionality, most of which are from the Scientific Data Reduction Benchmarks suite [17]. The datasets include 1) 1D HACC cosmology particle simulation [1], 2) 2D CESM-ATM climate simulation [27], 3) 3D Hurricane ISABEL simulation [28], 4) 3D Nyx cosmology simulation [29], 5) 3D seismic wave RTM data, 6) 3D hydrodynamics Miranda[30] (converted to float from double), and 6) 3D Quantum Monte Carlo [31], which is reinterpreted from 4D. They have been widely used in prior works [3, 4, 7, 32, 33] and are good representatives of production-level simulation datasets. TABLE IV shows all 128 fields across these datasets. The data sizes for the seven datasets are 6.3 GB, 2.0 GB, 1.9 GB, 3.0 GB, 1.8 GB, 1.0 GB, and 1.2 GB, respectively. Note that our evaluated HACC dataset is consistent with real-world scenarios that generate petabytes of data. For example, according to [1], a typical large-scale HACC simulation for cosmological surveys runs on 16,384 nodes each with 128 million particles and generates 5 PB over the whole simulation. The simulation contains 100 individual snapshots of roughly 3 GB per node. We evaluate a single snapshot for each dataset instead of all the snapshots, because the compressibility of most of the snapshots usually has strong similarity. Moreover, when the field is too large to fit in a single GPU's memory, CUSZ(x) divides it into blocks and then compresses by block.

B. Evaluation on Compression Ratio

TABLE V shows several cases that RLE performs better in compression ratio than CUSZ-VLE. Run-length encoding is implemented using `thrust::reduce_by_key` and achieves 100 GB/s throughput on V100 and slightly higher throughput on A100. The table demonstrates that RLE may replace the multibyte VLE in the original workflow and maintain or achieve higher compression ratios; it can be also used as an additional stage to VLE to get up to 5.3× compression ratio improvements over CUSZ on the tested datasets.

| datasets | dimensions | datum size | #fields |
|---------------------|-------------------|-------------------|--------------------|
| cosmology | | 1,071.75 MB | 6 in total |
| HACC | 280,953,867 | | x, vx |
| climate | | 24.72 MB | 77 in total |
| CESM-ATM | 1,800×3,600 | | CLDHGH, PHIS |
| climate | | 95.37 MB | 20 in total |
| Hurricane | 100×500×500 | | CLOUDf48, Uf48 |
| cosmology | | 512 MB | 6 in total |
| Nyx | 512×512×512 | | baryon_desnity |
| seismic wave | | 180.72 MB | 10 in total |
| RTM | 449×449×235 | | snapshot28{0...9}0 |
| hydrodynamics | | 144 MB | 7 in total |
| Miranda* | 256×384×384 | | density, pressure |
| Quantum Monte Carlo | | 601.52 MB | 2 in total |
| QMCPACK | 288x115x69x69 | | preconditioned |

TABLE IV: Real-world float-type datasets used in evaluation. Miranda (double-type) is converted to float-type for CUSZ’s sup-port. QMCPACK includes only one field but with two representations.

| | cuSZ+gzip | | ours | | ours | |
|-----------|------------------|----------|-------------|-------|-------------|-------|
| | (qhg) ref. | (qh) VLE | RLE | gain | RLE+VLE | gain |
| AEROD_v | 94.27 | 25.06 | 10.46 | - | 30.33 | 1.21× |
| FLNTC | 56.95 | 23.66 | 8.87 | - | 25.35 | 1.07× |
| FLUTC | 57.06 | 23.66 | 8.91 | - | 25.46 | 1.08× |
| FSDSC | 58.30 | 23.88 | 26.10 | 1.09× | 71.35 | 2.99× |
| FSDTOA | 430.61 | 26.10 | 43.65 | 1.67× | 119.17 | 4.57× |
| FSNSC | 51.73 | 23.44 | 10.11 | - | 29.46 | 1.26× |
| FSNTC | 60.35 | 23.88 | 12.33 | - | 35.50 | 1.49× |
| FSNTOAC | 111.63 | 25.06 | 12.46 | - | 35.84 | 1.43× |
| ICEFRAC | 159.18 | 25.31 | 16.57 | - | 50.39 | 1.99× |
| LANDFRAC | 97.15 | 23.66 | 13.98 | - | 40.50 | 1.71× |
| OCNFRAC | 89.55 | 23.88 | 11.23 | - | 32.55 | 1.36× |
| ODV_bcar1 | 189.28 | 25.83 | 37.28 | 1.44× | 110.51 | 4.28× |
| ODV_bcar2 | 197.32 | 25.83 | 30.71 | 1.19× | 89.98 | 3.48× |
| ODV_dust1 | 242.89 | 26.10 | 22.91 | - | 67.72 | 2.59× |
| ODV_dust2 | 319.55 | 26.37 | 24.02 | - | 70.98 | 2.69× |
| ODV_dust3 | 270.50 | 26.10 | 33.29 | 1.28× | 98.22 | 3.76× |
| ODV_dust4 | 230.40 | 26.10 | 46.81 | 1.79× | 139.27 | 5.34× |
| ODV_ocar1 | 65.81 | 24.11 | 41.17 | 1.71× | 121.59 | 5.04× |
| ODV_ocar2 | 64.92 | 24.11 | 33.79 | 1.40× | 98.63 | 4.09× |
| PHIS | 98.86 | 25.06 | 9.51 | - | 28.87 | 1.15× |
| PRECSC | 176.21 | 25.83 | 19.50 | - | 58.92 | 2.28× |
| PRECSL | 142.23 | 25.57 | 15.39 | - | 45.69 | 1.79× |
| PSL | 83.13 | 24.34 | 12.43 | - | 36.32 | 1.49× |
| PS | 98.59 | 21.09 | 7.45 | - | 22.27 | 1.06× |
| SNOWHICE | 144.74 | 25.31 | 15.14 | - | 45.53 | 1.80× |
| SNOWHIND | 184.39 | 25.57 | 21.18 | - | 63.33 | 2.48× |
| SOLIN | 430.62 | 26.10 | 43.65 | 1.67× | 119.17 | 4.57× |
| TAUX | 100.30 | 25.06 | 11.30 | - | 33.28 | 1.33× |
| TAUY | 106.55 | 25.31 | 12.40 | - | 36.45 | 1.44× |
| TREFHT | 82.50 | 24.58 | 8.75 | - | 25.12 | 1.02× |
| TREFMXAV | 87.39 | 24.58 | 9.60 | - | 27.33 | 1.11× |
| TROP_P | 93.78 | 24.82 | 11.19 | - | 31.40 | 1.27× |
| TROP_T | 92.94 | 24.82 | 11.10 | - | 30.64 | 1.23× |
| TROP_Z | 84.81 | 24.58 | 9.48 | - | 27.07 | 1.10× |
| TSMX | 64.95 | 23.88 | 8.55 | - | 24.69 | 1.03× |

TABLE V: Data fields that CUSZ(x) with RLE-based compression workflow has higher compression ratio than CUSZ with VLE-only compression workflow under 10^{-2} error bound. The compression ratio gain of our solution is against (qh) VLE from CUSZ.

TABLE VI shows the throughputs of CUSZ(x) using the RLE-based compression workflow on the RTM, CESM, and Nyx datasets. It demonstrates that the RLE-based workflow can not only improve the compression ratio but also maintain a comparable compression throughput. Therefore, CUSZ(x) can

| | | V100 (GB/s) | | A100 (GB/s) | | CR |
|-------------------|------|--------------------|---------|--------------------|---------|---------------|
| | | Huff/RLE | overall | Huff/RLE | overall | |
| RTM #2800 | ours | 142.4 | 57.8 | 212.6 | 78.0 | 76.0× |
| | cuSZ | 135.7 | 55.1 | 233.9 | 80.8 | 31.7× |
| CESM FSDSC | ours | 104.8 | 47.7 | 162.4 | 57.8 | 26.1× |
| | cuSZ | 146.3 | 54.8 | 146.4 | 55.5 | 23.0× |
| Nyx baryon | ours | 159.1 | 64.1 | 214.5 | 91.2 | 122.7× |
| | cuSZ | 130.8 | 58.9 | 234.2 | 94.8 | 31.0× |

TABLE VI: Throughputs (in GB/s) of CUSZ(x) (based on RLE) and CUSZ (based on Huffman coding) on example RTM, CESM, and Nyx fields for demonstration purpose.

provide users a flexibility between high compression ratio and high compression performance.

C. Evaluation on Performance and Scalability

In this section, we evaluate the compression performance of CUSZ(x) and compare it with CUSZ.

1) *Evaluation on Optimized Kernels*: We first evaluate the performance of the majorly changed kernels in CUSZ(x) and CUSZ on V100, as shown in TABLE VII. The baseline is from the evaluation results shown in the CUSZ paper [13]. The table illustrates that the performance improvements of CUSZ(x)’s Lorenzo construction kernel are $1.48\times$ for 1D data, $1.09\times$ for 2D data, and $1.45\times$ for 3D data on average over CUSZ. Moreover, we increase the lowest throughput from 175.8 GB/s to 229.9 GB/s (+30.7%) on the tested datasets.

For Huffman encoding kernel, despite it is more latency-bound, it also suffers from non-coalescing store. Because of the variable length encoding and bit operation spanning multiple bytes, it is impossible to make threads work in a synchronized manner (otherwise, a high synchronization overhead would be imposed). Our optimization can decrease the number of DRAM store transactions to be inversely proportional to the compression ratio. In particular, we perform a DRAM store only when a new data unit needs to write back, which helps us achieve $1.08\times\sim 2.05\times$ performance gain.

The table also shows that, by using the fine-grained ND partial-sum computation, CUSZ(x)’s Lorenzo reconstruction kernel exhibits up to $18.4\times$ performance improvements over CUSZ’s coarse-grained kernel. The 2D and 3D kernels also exhibit $4.5\times$ and $4.6\sim 7.1\times$ performance improvements, respectively. In addition, TABLE VIII shows the speedup of our optimized kernels on A100 compared to on V100.

2) *Evaluation on Default Compression Workflow*: The rest of TABLE VIII shows the performance evaluation of CUSZ(x) based on the default compression workflow on both V100 and A100 with the relative error bound of 10^{-4} (with PSNRs higher than 85 dB). It illustrates the performance of our optimized compression and decompression kernels. We note that the performance improvements of the histogram kernel and the gather outlier kernel are relatively lower than those of other compression kernels (the performance is even degraded on some datasets such as CESM and RTM) from using A100 to using V100. This may be because each field of CESM-ATM and RTM is fairly small (~ 25 MB and 180 MB, respectively), such that the histogram kernel (using the xxx algorithm) and the gather outlier kernel (using the dense-to-sparse kernel from cuSPARSE) on A100 do not maintain the same work efficiency

| | Lorenzo comp. | | | Huffman Enc. | | Lorenzo decomp. | | | |
|-----------|----------------------|-------|--------------|---------------------|-------|------------------------|------|-------|---------------|
| | cuSZ | ours | | cuSZ | ours | cuSZ | ours | | |
| HACC | 207.7 | 307.4 | 1.48× | 54.1 | 58.3 | 1.08× | 16.8 | 313.1 | 18.64× |
| CESM | 252.1 | 273.9 | 1.09× | 57.2 | 107.7 | 1.88× | 58.5 | 254.2 | 4.35× |
| Hurricane | 175.8 | 229.9 | 1.31× | 55.2 | 111.2 | 2.01× | 43.9 | 218.4 | 4.97× |
| Nyx | 200.2 | 296.0 | 1.48× | 58.8 | 120.5 | 2.05× | 29.7 | 238.1 | 8.02× |
| QMCPACK | 189.6 | 298.6 | 1.57× | 61.0 | 110.8 | 1.82× | 22.4 | 255.5 | 11.41× |

TABLE VII: Performance comparison of Lorenzo and Huffman encoding kernels in CUSZ(x) and CUSZ on V100.

| size in MB | V100-ours, GB/s | | | | | | | A100-ours, GB/s (and advantage over V100) | | | | | | | | | | | | | |
|------------------|-----------------|-------------|-------------|------------|------------|--------------|------------|---|-------------|-------------|------------|------------|----------------|------------|-------|-------|-------|--------|-------|-------|-------|
| | 1071.8 | 24.7 | 95.4 | 512.0 | 180.7 | 144.0 | 601.5 | 1071.8 | 24.7 | 95.4 | 512.0 | 180.7 | 144.0 | 601.5 | | | | | | | |
| | HACC | CESM | Hurr | Nyx | RTM | Mira. | QMC | HACC | CESM | Hurr | Nyx | RTM | Miranda | QMC | | | | | | | |
| Lorenzo const | 328.3 | 273.9 | 199.0 | 296.0 | 193.1 | 289.3 | 298.6 | 501.1 | 1.53× | 466.8 | 1.70× | 429.0 | 2.16× | 481.3 | 1.63× | 422.7 | 2.19× | 480.7 | 1.66× | 492.9 | 1.65× |
| gather outlier | 221.4 | 160.6 | 251.1 | 238.0 | 249.7 | 228.6 | 261.2 | 324.8 | 1.47× | 151.4 | 0.94× | 284.2 | 1.13× | 334.9 | 1.41× | 221.6 | 0.89× | 336.0 | 1.47× | 266.2 | 1.02× |
| histogram | 565.9 | 356.5 | 438.4 | 372.4 | 573.6 | 489.8 | 724.3 | 923.5 | 1.63× | 409.8 | 1.15× | 681.2 | 1.55× | 870.2 | 2.34× | 793.9 | 1.38× | 714.9 | 1.46× | 569.7 | 0.79× |
| Huffman enc. | 58.3 | 107.7 | 111.2 | 120.5 | 123.2 | 161.1 | 110.8 | 174.6 | 2.99× | 121.6 | 1.13× | 206.0 | 1.85× | 217.2 | 1.80× | 202.2 | 1.64× | 201.6 | 1.25× | 198.4 | 1.79× |
| comp. overall | 42.1 | 44.8 | 49.3 | 53.9 | 52.5 | 62.2 | 56.9 | 84.1 | 2.00× | 51.5 | 1.15× | 82.2 | 1.67× | 92.4 | 1.72× | 76.4 | 1.46× | 87.6 | 1.41× | 79.5 | 1.40× |
| Huffman dec. | 42.1 | 37.9 | 45.8 | 66.8 | 48.9 | 42.7 | 44.6 | 48.5 | 1.15× | 26.6 | 0.70× | 51.8 | 1.13× | 91.2 | 1.37× | 56.0 | 1.15× | 50.1 | 1.17× | 49.0 | 1.10× |
| scatter outlier | 225.0 | 334.8 | 628.1 | 359.7 | 440.2 | 679.1 | 347.1 | 658.4 | 2.93× | 630.2 | 1.88× | 918.3 | 1.46× | 797.4 | 2.22× | 906.6 | 2.06× | 1066.8 | 1.57× | 782.8 | 2.26× |
| Lorenzo reconst. | 308.7 | 267.0 | 200.1 | 251.7 | 201.3 | 245.3 | 255.5 | 504.4 | 1.63× | 495.3 | 1.86× | 345.5 | 1.73× | 398.6 | 1.58× | 335.6 | 1.67× | 386.9 | 1.58× | 384.0 | 1.50× |
| decomp. Overall | 31.8 | 30.2 | 35.2 | 46.0 | 36.1 | 34.5 | 34.2 | 41.4 | 1.30× | 24.3 | 0.80× | 43.0 | 1.22× | 67.9 | 1.47× | 45.6 | 1.26× | 42.6 | 1.23× | 41.2 | 1.20× |

TABLE VIII: Evaluation of CUSZ(x) using default compression workflow (Lorenzo and multibyte VLE) with relative error bound of 10^{-4} on V100 and A100: breakdown throughput of compression subprocedures.

as on V100. But, it is worth noting that these two kernels would not be bottlenecks⁴ for a relatively large dataset (e.g., hundreds of MBs per field), which is more common in practice (e.g., HACC and Nyx).

In addition, we observe that CUSZ(x)’s kernels with different parallelism have different scalabilities. Specifically, the sparsity-relation operation in compression can be significantly enhanced by using A100 GPU, but the performance of other compression kernels such as Huffman encoding are scaled up marginally. As a result, the overall compression performance improvement is limited when changing from using V100 to using A100. Similarly, for decompression, although the outlier scatter operation scales naturally and shows a speedup of higher than 2×, the multibyte Huffman decoding exhibits a stagnation in scaling up, resulting in a marginal improvement of the overall decompression performance.

VI. RELATED WORK

Compression for scientific datasets has been studied for years, in order to reduce the storage burden and I/O overhead. Basically, scientific data compression techniques can be categorized into two classes: lossless compression and lossy compression. The former includes the generic lossless compressors such as Zlib [34] and Zstd [18], as well as the specific algorithm designed for floating-point values such as FPZIP [35] and FPC [36]. The lossless compressors, however, all suffer from very low compression ratios (generally $\sim 2:1$ or even lower [6]) because of the rather random ending mantissa bits in the floating-point representation.

Lossy compressors have been studied for decades. The traditional lossy compressors (such as JPEG [37] and JPEG2000 [38]) are designed for 2D images, which are not suitable for scientific datasets. The key reason is that the traditional lossy compressors focus on the visual quality while scientific applications care more about the post hoc analysis results, which is beyond the simple visualization purpose.

To address the above-mentioned gap, error-bounded lossy compressors [8, 9, 10, 11, 39] have been proposed for years. Based on their design principle, they can be split into two categories - prediction-based model [3, 8, 9] and transform-based model [10, 39, 40]. The typical example in the former category is SZ, which supports different types of errors to

⁴The Huffman encoding kernel is the main bottleneck in the compression workflow compared to other compression kernels.

control data distortion such as absolute error bound, relative error bound and peak signal-to-noise ratio (PSNR). The typical example in the latter category is ZFP, which supports absolute error bound and precision mode⁵.

However, all the above existing lossless and lossy compressors cannot run on GPUs directly. Recently, both the SZ team and the ZFP team released their CUDA versions, called CUSZ [13] and cuZFP [14], respectively. Both versions provide much higher throughputs for compression and decompression compared with their CPU versions. Compared with CUSZ, cuZFP provides slightly higher compression throughput, but it only supports fixed-rate mode, which significantly limits its adoption in practice. In comparison with the two existing GPU-supported compressors, our designed new compression method is aware of the incompressibility of the datasets, such that it can adopt the run-length encoding (RLE) method to significantly improve the compression ratios when needed.

VII. CONCLUSION AND FUTURE WORK

In this work, we propose CUSZ(x), a compressibility-aware GPU-based lossy compressor for NVIDIA GPU architectures, which can effectively improve the compression throughput over CUSZ. Specifically, we propose an efficient compression method to adaptively perform run-length encoding and/or Huffman encoding by considering data sparsity and smoothness to improve the compression ratio of CUSZ. We prove that the Lorenzo reconstruction in decompression is equivalent to a multidimensional partial-sum computation and develop an efficient fine-grained Lorenzo reconstruction algorithm on GPUs. Moreover, we carefully optimize CUSZ’s compression kernels leveraging the state-of-the-art NVIDIA cub parallel primitives in CUDA architectures. Finally, we evaluate CUSZ(x) using seven real-world HPC application datasets on the most advanced GPUs (V100 and A100) and compare with other state-of-the-art lossy compression methods. Experiments show that our CUSZ(x) improves CUSZ’s decompression kernel throughput by up to 1.6× with the same compression quality on state-of-the-art GPUs including NVIDIA A100.

In the future, we plan to further optimize the performance of decompression, implement other data prediction methods such as linear-regression-based predictor, and evaluate the performance improvements of parallel I/O with CUSZ.

⁵In the precision mode, users can use an integer number to control the data distortion. Higher precision value means lower data distortion.

REFERENCES

- [1] S. Habib, V. Morozov, N. Frontiere, H. Finkel, A. Pope, K. Heitmann, K. Kumaran, V. Vishwanath, T. Peterka, J. Insley, *et al.*, “HACC: Extreme scaling and performance across diverse architectures,” *Communications of the ACM*, vol. 60, no. 1, pp. 97–104, 2016.
- [2] S. C. V. Vishwanath and K. Harms, *Parallel i/o on mira*, https://www.alcf.anl.gov/files/Parallel_IO_on_Mira_0.pdf, Online, 2019.
- [3] X. Liang, S. Di, D. Tao, S. Li, S. Li, H. Guo, Z. Chen, and F. Cappello, “Error-controlled lossy compression optimized for high compression ratios of scientific datasets,” in *2018 IEEE International Conference on Big Data (Big Data)*, Seattle, WA, USA: IEEE, 2018, pp. 438–447.
- [4] X. Liang, S. Di, D. Tao, Z. Chen, and F. Cappello, “An efficient transformation scheme for lossy data compression with point-wise relative error bound,” in *IEEE International Conference on Cluster Computing (CLUSTER)*, Belfast, UK: IEEE, 2018, pp. 179–189.
- [5] D. Meister, J. Kaiser, A. Brinkmann, T. Cortes, M. Kuhn, and J. Kunkel, “A study on data deduplication in HPC storage systems,” in *SC '12: Proceedings of the International Conference on High Performance Computing, Networking, Storage and Analysis*, Salt Lake City, UT, USA: IEEE, 2012, p. 7.
- [6] S. W. Son, Z. Chen, W. Hendrix, A. Agrawal, W.-k. Liao, and A. Choudhary, “Data compression for the exascale computing erasurvey,” *Supercomputing Frontiers and Innovations*, vol. 1, no. 2, pp. 76–88, 2014.
- [7] F. Cappello, S. Di, S. Li, X. Liang, A. M. Gok, D. Tao, C. H. Yoon, X.-C. Wu, Y. Alexeev, and F. T. Chong, “Use cases of lossy compression for floating-point data in scientific data sets,” *The International Journal of High Performance Computing Applications*, vol. 33, no. 6, pp. 1201–1220, 2019.
- [8] S. Di and F. Cappello, “Fast error-bounded lossy HPC data compression with SZ,” in *2016 IEEE International Parallel and Distributed Processing Symposium*, Chicago, IL, USA: IEEE, 2016, pp. 730–739.
- [9] D. Tao, S. Di, Z. Chen, and F. Cappello, “Significantly improving lossy compression for scientific data sets based on multidimensional prediction and error-controlled quantization,” in *2017 IEEE International Parallel and Distributed Processing Symposium*, Orlando, FL, USA: IEEE, 2017, pp. 1129–1139.
- [10] P. Lindstrom, “Fixed-rate compressed floating-point arrays,” *IEEE Transactions on Visualization and Computer Graphics*, vol. 20, no. 12, pp. 2674–2683, 2014.
- [11] P. Lindstrom and M. Isenburg, “Fast and efficient compression of floating-point data,” *IEEE Transactions on Visualization and Computer Graphics*, vol. 12, no. 5, pp. 1245–1250, 2006. <https://lcls.slac.stanford.edu/lasers/lcls-ii>, Online.
- [12] J. Tian, S. Di, K. Zhao, C. Rivera, M. H. Fulp, R. Underwood, S. Jin, X. Liang, J. Calhoun, D. Tao, *et al.*, “Cusz: An efficient gpu-based error-bounded lossy compression framework for scientific data,” in *Proceedings of the ACM International Conference on Parallel Architectures and Compilation Techniques*, 2020, pp. 3–15.
- [13] cuZFP, https://github.com/LLNL/zfp/tree/develop/src/cuda_zfp, Online, 2019.
- [14] J. Tian, C. Rivera, S. Di, J. Chen, X. Liang, D. Tao, and F. Cappello, “Revisiting huffman coding: Toward extreme performance on modern gpu architectures,” in *2021 IEEE International Parallel and Distributed Processing Symposium (IPDPS)*, Portland, OR, USA, May 17–21, 2021, IEEE, 2021, pp. 881–891.
- [15] *Nvidia/cub: Cooperative primitives for cuda c++*. <https://github.com/NVIDIA/cub>.
- [16] Scientific Data Reduction Benchmarks, <https://sdrbench.github.io/>, Online, 2019.
- [17] Zstd, <https://github.com/facebook/zstd/releases>, Online, 2019.
- [18] K. Zhao, S. Di, M. Dmitriev, T.-L. D. Tonellot, Z. Chen, and F. Cappello, “Optimizing error-bounded lossy compression for scientific data by dynamic spline interpolation,” in *2021 IEEE 37th International Conference on Data Engineering (ICDE)*, IEEE, 2021, pp. 1643–1654.
- [19] *Nvcomp*, <https://github.com/NVIDIA/nvcomp>, (Accessed on 05/19/2021).
- [20] A. H. Robinson and C. Cherry, “Results of a prototype television bandwidth compression scheme,” *Proceedings of the IEEE*, vol. 55, no. 3, pp. 356–364, 1967. DOI: 10.1109/PROC.1967.5493.
- [21] O. Johnsen, “On the redundancy of binary huffman codes (corresp.),” *IEEE Transactions on Information Theory*, vol. 26, no. 2, pp. 220–222, 1980, ISSN: 1557-9654. DOI: 10.1109/TIT.1980.1056158.
- [22] R. Gallager, “Variations on a theme by huffman,” *IEEE Transactions on Information Theory*, vol. 24, no. 6, pp. 668–674, 1978. DOI: 10.1109/TIT.1978.1055959.
- [23] N. Cressie and D. M. Hawkins, “Robust estimation of the variogram: I,” *Journal of the International Association for Mathematical Geology*, vol. 12, no. 2, pp. 115–125, 1980.
- [24] *Theta/thetagpu - argonne leadership computing facility*, <https://www.alcf.anl.gov/support-center/theta/theta-thetagpu-overview>, (Accessed on 05/21/2021).
- [25] *Longhorn - texas advanced computing center*, <https://www.tacc.utexas.edu/systems/longhorn>, (Accessed on 03/15/2021).
- [26] Community Earth System Model (CESM) Atmosphere Model, <http://www.cesm.ucar.edu/models/>, Online, 2019.
- [27] Hurricane ISABEL Simulation Data, <http://vis.computer.org/vis2004contest/data.html>, Online, 2019.
- [28] NYX simulation, <https://amrex-astro.github.io/Nyx/>, Online.
- [29] Miranda Radiation Hydrodynamics Data, <https://wci.llnl.gov/simulation/computer-codes/miranda>, Online, 2019.
- [30] QMCPACK: many-body ab initio Quantum Monte Carlo code, <http://vis.computer.org/vis2004contest/data.html>, Online, 2019.
- [31] D. Tao, S. Di, X. Liang, Z. Chen, and F. Cappello, “Optimizing lossy compression rate-distortion from automatic online selection between SZ and ZFP,” *IEEE Transactions on Parallel and Distributed Systems*, vol. 30, no. 8, pp. 1857–1871, 2019.
- [32] X. Liang, S. Di, D. Tao, S. Li, B. Nicolae, Z. Chen, and F. Cappello, “Improving performance of data dumping with lossy compression for scientific simulation,” in *2019 IEEE International Conference on Cluster Computing (CLUSTER)*, Albuquerque, NM, USA: IEEE, 2019, pp. 1–11.
- [33] L. P. Deutsch, *GZIP file format specification version 4.3*, 1996.
- [34] P. Lindstrom and M. Isenburg, “Fast and efficient compression of floating-point data,” *IEEE Transactions on Visualization and Computer Graphics*, vol. 12, no. 5, pp. 1245–1250, 2006.
- [35] M. Burtcher and P. Ratanaworabhan, “FPC: A high-speed compressor for double-precision floating-point data,” *IEEE Transactions on Computers*, vol. 58, no. 1, pp. 18–31, 2008.
- [36] G. K. Wallace, “The JPEG still picture compression standard,” *IEEE Transactions on Consumer Electronics*, vol. 38, no. 1, pp. xviii–xxxiv, 1992.
- [37] D. Taubman and M. Marcellin, *JPEG2000 image compression fundamentals, standards and practice: image compression fundamentals, standards and practice*. Boston, MA, USA: Springer Science & Business Media, 2012, vol. 642.
- [38] N. Sasaki, K. Sato, T. Endo, and S. Matsuoka, “Exploration of lossy compression for application-level checkpoint/restart,” in *2015 IEEE International Parallel and Distributed Processing Symposium (IPDPS)*, Hyderabad, India: IEEE, 2015, pp. 914–922.
- [39] J. Clyne, P. Mininni, A. Norton, and M. Rast, “Interactive desktop analysis of high resolution simulations: Application to turbulent plume dynamics and current sheet formation,” *New Journal of Physics*, vol. 9, no. 301, pp. 1–29, 2007.